Ion Thermal Confinement in the Enhanced-Confinement Regime of the TFTR Tokamak

R. J. Fonck, R. Howell,[a] K. Jaehnig, L. Roquemore, G. Schilling, S. Scott, M. C. Zarnstorff, C. Bush, R. Goldston, H. Hsuan, D. Johnson, A. Ramsey, J. Schivell, and H. Towner

Princeton Plasma Physics Laboratory, Princeton, New Jersey 08543

(Received 14 October 1988)

Central ion temperatures up to 30 keV and rotation speeds up to 8×10^5 m/sec have been confirmed with new diagnostic measurements in the TFTR hot-ion enhanced-confinement regime, and the ion thermal diffusivity is found to be non-neoclassical and comparable to the anomalous electron thermal diffusivity. The dominant effect of strong rotation is the downshifting of the neutral beam energies in the plasma frame, which results in reduced ion and electron heating on axis, and the presence of off-axis ion heating from viscous damping of the plasma rotation.

PACS numbers: 52.50.Gj, 28.50.Re, 52.55.Fa

Central-ion-temperature measurements on early smaller tokamaks and the lack of good profile information led to a common assumption that the plasma ion thermal transport was reasonably described by a thermal diffusivity, χ_i, whose magnitude was typically up to a few times that predicted by neoclassical theory coupled with a convective power flux $=\frac{5}{2}n_iT_iv_\perp$. As a consequence, ion thermal energy transport was not considered to be a dominant loss channel in neutral-beam-heated plasmas.[1-4] With the development of the charge-exchange recombination spectroscopy technique to provide reliable measurements of the ion-temperature profile, this interpretation has come into question.[5,6] It is thus interesting to study ion thermal confinement in the present generation of large, high-temperature tokamak experiments. The enhanced-confinement regime[7] of the TFTR tokamak offers an especially attractive environment for such ion power-balance studies in large tokamak experiments since the high electron temperatures and modest densities attained here result in almost negligible ion-electron coupling, and ion thermal conduction is the dominant ion energy-loss mechanism over most of the plasma cross section.

The high-temperature enhanced-confinement ("supershot") regime is attained in TFTR by neutral beam injection into a low-recycling target plasma. The discharges studied here had a major radius of 2.45 m and a minor radius of 0.79 m. Deuterium plasmas were heated by up to 20 MW of deuterium neutral beam injection, with about 6 MW countertangential to the plasma current, and the remaining power cotangential. The highest values of stored energy, central ion temperature, and neutron emission were obtained with near-balanced injection.[8] With the availability of up to ≈ 12 MW of balanced beam power, maximum temperatures and neutron output were attained at discharge currents of 0.8 to 1.0 MA. The ion-temperature profiles were highly peaked for the balanced-injection cases, while they were broader for the lower-confinement, purely coinjection cases with high toroidal rotation speeds, as was also the case for the measured electron-density profiles.

A multispatial and multispectral imaging charge-exchange recombination spectroscopy (CHERS) diagnostic was installed on TFTR to provide radially resolved measurements of the ion temperature, $T_i(R,t)$, and toroidal rotation speed, $v_\varphi(R,t)$, for a wide range of discharge parameters. For most of the measurements reported here, the C VI 5292-Å ($n=8$–7) transition was used.[9] The central values of T_i and v_φ in the enhanced-confinement regime measured by the CHERS diagnostic and by x-ray Doppler-broadening measurements of the Ni XXVII $K\alpha$ line are in agreement within their respective error bars.[8,10]

The measured profiles have been analyzed with the SNAP (1D, equilibrium) and TRANSP ($1\frac{1}{2}$D, time-dependent) kinetic analysis codes, with an emphasis on deriving the ion thermal diffusivities and elucidating the effects of rotation on the thermal ion power balance. These codes use, among other parameters, the measured profiles of ion and electron temperature, electron density, and plasma toroidal rotation speed to derive the power balance for each plasma species. Both codes can be used in either an analysis mode, in which the measured $T_i(r)$ profiles are used as input to derive a value of $\chi_i(r)$ from the data, or in a predictive mode, in which a given model is chosen for $\chi_i(r)$ and the resulting calculated $T_i(r)$ profile is compared to the measurements. In these kinetic analyses, we assume classical electron-ion coupling and a spatially uniform $Z_{\rm eff}$ profile. The assumption of a flat $Z_{\rm eff}$ profile is supported by visible continuum measurements of $Z_{\rm eff}$ and CHERS measurements of C^{+6} densities in similar supershot discharges.

Comparisons of the measured $T_i(r)$ profiles with model transport calculations from SNAP in the predictive mode show that the ion thermal diffusion is strongly nonneoclassical. For example, Fig. 1(a) shows the measured $T_i(r)$ profile for a 0.9-MA discharge with 13.6 MW of balanced neutral injection, $\bar{n}_e=2.5\times10^{19}$ m^{-3} and $n_e(0)=5.0\times10^{19}$ m^{-3}. The data, indicated by the solid squares in the plot, include values obtained for $r/a<0.3$

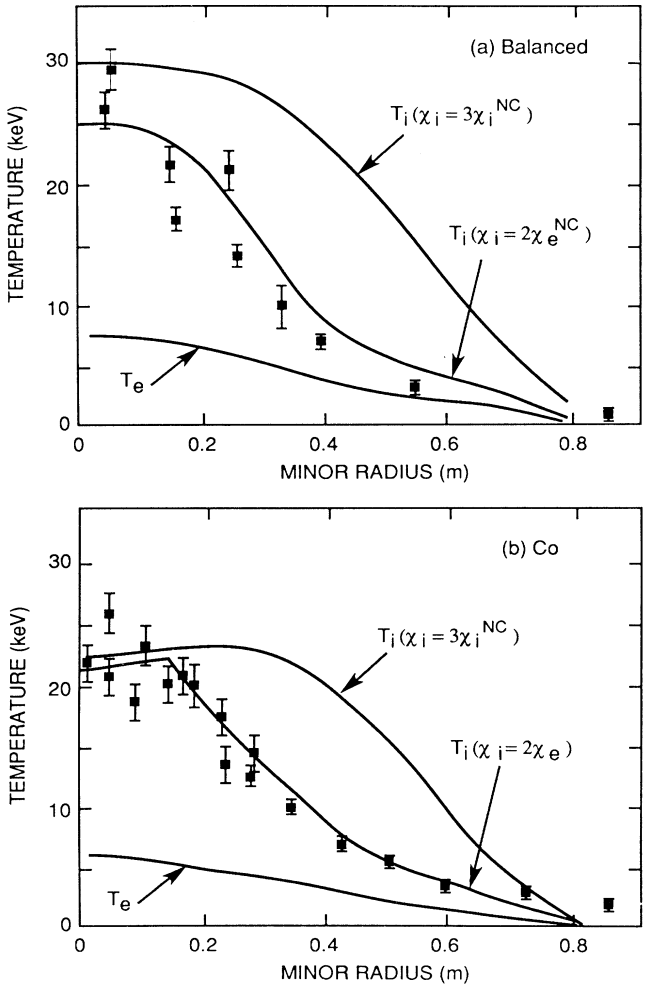

FIG. 1. (a) Measured and simulated ion-temperature profiles for a balanced-injection discharge. The smoothed T_e profile is also shown. (b) Same as (a) but for full coinjection with $v_\varphi(0) = 8\times10^5$ m/sec.

from both the inboard and outboard sides of the plasma with respect to the magnetic axis, while data were available only from the outboard plasma side for $r/a > 0.3$. Also shown in Fig. 1(a) are comparisons of the measured $T_i(r)$ profile with the values calculated from the SNAP code under the assumptions that $\chi_i = 3\chi_i^{NC}$, where χ_i^{NC} is the Chang-Hinton neoclassical ion thermal diffusivity,[11] and $\chi_i(r) = 2\chi_e(r)$, where $\chi_e(r)$ is the electron thermal diffusivity derived from the measured $T_e(r)$ profiles. The measured $T_i(r)$ profile is clearly much narrower than that expected from neoclassical theory, while $\chi_i \approx 2\chi_e$ produces a much closer approximation to the measured values. Indeed, a survey of several discharges using the SNAP code in the analysis mode to derive a $\chi_i(R)$ profile indicates that $\chi_i \approx (1\text{-}3)\chi_e$ at $r/a \approx 0.5$-0.7, with similar radial profiles except in the innermost central region. More detailed modeling with the TRANSP code for a wide range of discharges indicates that $\chi_i \approx 2\chi_e$ is often a reasonable approximation for most of the plasma cross section, but the actual value of the multiplier can vary with the degree of peaking of the density profile. The measured values of $\eta_i^{tot} = L_{ni}^{tot}/L_{ti}$, where L_{ni}^{tot} is the total-ion density-gradient scale length and L_{ti} is the thermal-ion temperature-gradient scale length, usually lie within the range of $\eta_i^{tot} = 2 \pm 1$ for $a/4 < r < a/2$.[12]

While ion thermal convection is usually negligible over most of the minor radius, it is significant in the central plasma region ($r/a < 0.2$). Depending on the discharge conditions, a convective ion power flow given by $Q_{i,conv} \approx 1.5 T_i \Gamma_i$ (where Γ_i is the ion particle flux) is required to give good agreement with the measured profiles and to avoid unphysical negative χ_i's in the central plasma region. The deviation of the convective multiplier from the often-used value of $\frac{5}{2}$ presumably reflects the nature of the assumed turbulence underlying this convective transport.[13] For consistency, we use a value of $\frac{3}{2}$ in the analyses presented here.

High toroidal rotation speeds have a direct influence on the plasma performance in this hot-ion regime, and measurements of the T_i and v_φ radial profiles help to quantify the effects of rotation on the plasma behavior. The overall neutron yield is lowered by the reduced relative energy between the fast ions and the rotating bulk plasma ions, and rotation has a strong effect on the plasma power deposition.[14] The reduced relative speeds between the plasma and neutral beam particles results in reduced beam energy deposited in the plasma in its rotating frame, and reduced beam penetration to the plasma core. This in turn results in a power-deposition profile with less central ion and electron heating than in the nonrotating case. The viscous damping of the plasma rotation is assumed to provide an additional source of heating power to the ions which, since it is strongest where the $v_\varphi(r)$ gradient is largest, peaks off axis.

These combined effects of rotation lead to the broader $T_i(r)$ profiles observed in unbalanced-injection cases, and, in extreme cases, have resulted in flat or hollow $T_i(r)$ profiles. For example, Fig. 1(b) shows the measured and calculated ion-temperature profiles for an unbalanced-injection case. Here, full coinjection of 11 MW gives rise to a peaked $v_\varphi(r)$ profile (i.e., Gaussian in shape with a half width at half maximum ≈ 0.34 m) with $v_\varphi(0) \approx 8\times10^5$ m/sec for a standard 0.9-MA discharge of $\bar{n}_e = 1.7\times10^{19}$ m^{-3} and $n_e(0) = 3.1\times10^{19}$ m^{-3}. As with the balanced-injection case, the ion thermal diffusivity χ_i is strongly non-neoclassical, and $\chi_i \sim \chi_e$ plus the effects of ion viscous heating reasonably reproduces the measured $T_i(r)$ profile. The analysis of the momentum transport in these plasmas will be reported discharge, estimated from the uncertainties in the $T_i(r)$, $T_e(r)$, Z_{eff}, and other parameters from a single shot, are

ed in a separate paper.[15]

Figures 2(a)–2(d) show the calculated heating-power-density profiles and the integrated power-balance profiles for both the balanced-injection and the fully coinjected discharges discussed above. To ease comparison between these different cases, we plot here the power densities divided by the volume-averaged total input heating power from the neutral beams (i.e., the absorbed beam power minus direct charge-exchange ion losses). Likewise, the ion power-balance curves from SNAP shown in Figs. 2(c) and 2(d) give the volume-integrated power losses normalized to the total heating power. In the balanced-injection case, the high relative beam energies lead to substantial direct ion and electron heating in the plasma center and strong central absorption of the neutral beams in these low-recycling, low-edge-density discharges. In contrast, the downshifted relative beam energies in the rotating-plasma case lead to reduced central heating of the ions and electrons and a somewhat broadened beam-deposition profile. In addition, there is substantial off-axis heating of the ions due to viscous rotation damping.

The ion power balance for the balanced-injection case confirms that the ion power losses are strongly dominated by thermal conduction (given by $n_i\chi_i\nabla T_i$) over most of the plasma cross section, except for the central $r/a \leq 0.2$ region, where conductive and convective losses are of equal magnitude. In some contrast, the ion power-balance analysis of the rotating plasma [Fig. 2(d)] indicates that convection dominates the core power flow for $r/a \leq 0.3$, and it remains non-negligible (along with electron-ion coupling) beyond $r/a \approx 0.6$. The volume-integrated power input to the ions from viscous damping of the plasma rotation becomes a significant fraction of the overall input power to the ions for $r > 0.4$ m. In both cases, the consequence of $\chi_i(r) \approx \chi_e(r)$ is that the ion loss channels are much more important in the overall power balances than for the case of neoclassical transport.

Figure 3 shows the comparisons of the inferred $\chi_i(r)$ and $\chi_e(r)$ for four balanced- ($\tau_E = 0.13$ sec) and two unbalanced- ($\tau_E = 0.10$ sec) injection cases. These shots had 0.9 MA, with $P_{inj} \approx 11$ MW for the coinjection cases, and 12–14 MW for the balanced cases. The results are plotted in Fig. 3 as a range of values of χ at each radius, with the range indicating the spread of values obtained from the similar discharges. The uncertainties in the values of $\chi_i(r)$ and $\chi_e(r)$ from a single

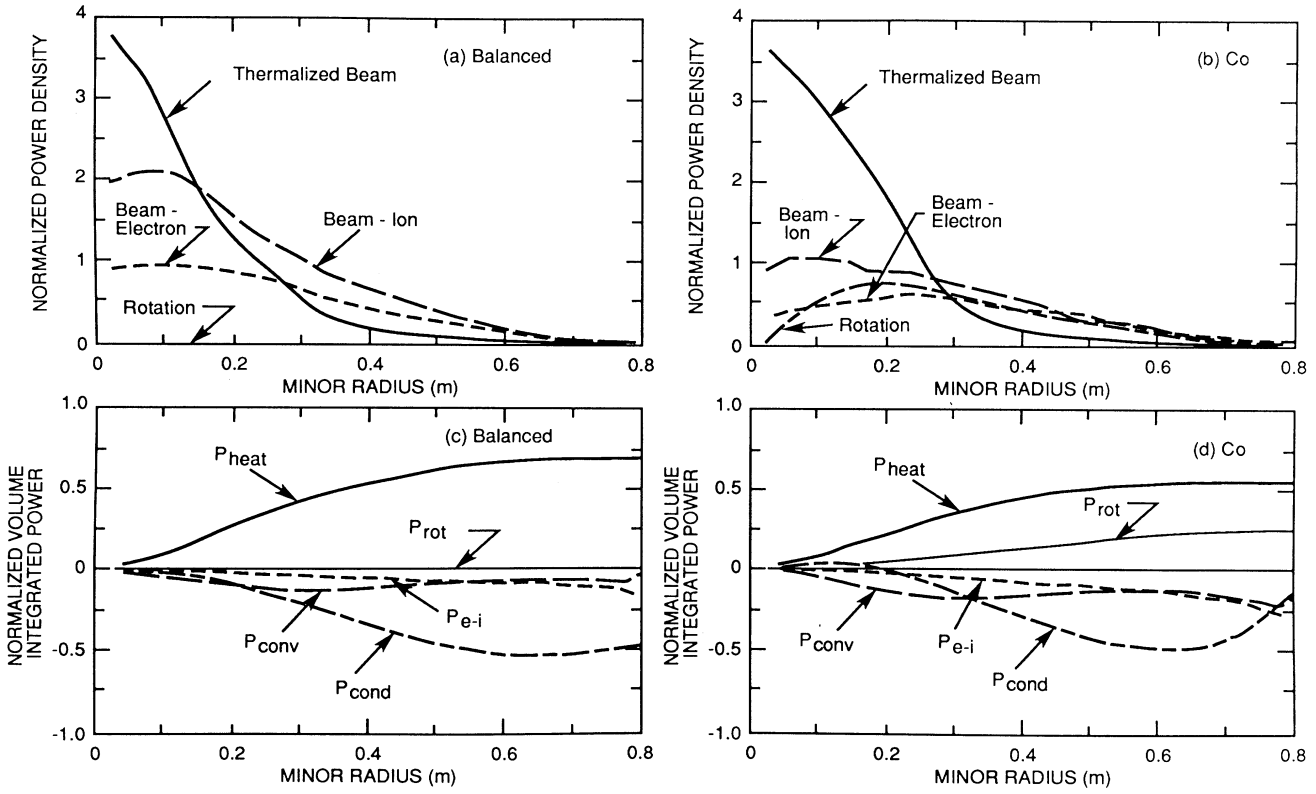

FIG. 2. Comparison of input power densities and volume-integrated ion power balance for a nonrotating and strongly rotating discharge. (a), (c) For the balanced case, $P_{inj} = 13.6$ MW and $P_{absorbed} = 12.8$ MW; (b), (d) $P_{inj} = 11.0$ MW and $P_{absorbed} = 10.4$ MW.

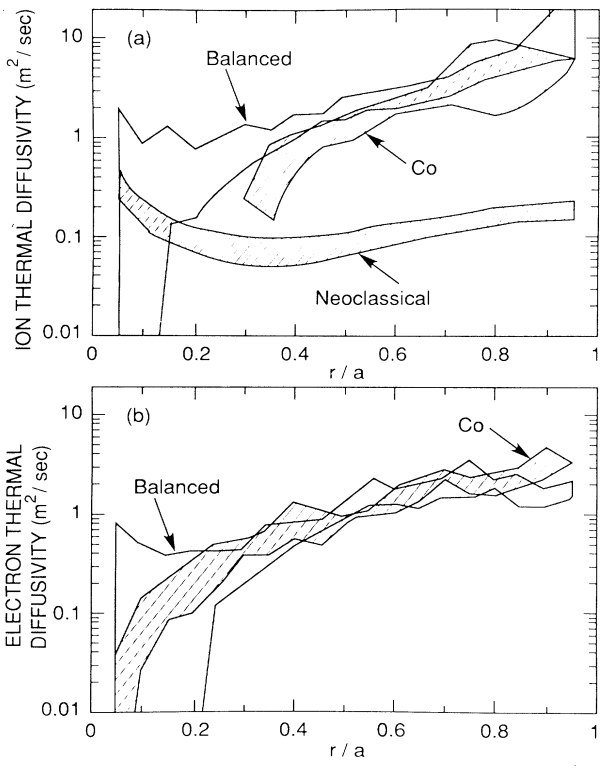

FIG. 3. (a) Ion and (b) electron thermal diffusivities for nonrotating and rotating discharges. The neoclassical ion diffusivity range includes both types of discharges.

1 to 2 times larger than the ranges indicated in Fig. 3 for $r/a \geq 0.5$. At small radii, near the plasma center, large uncertainties in χ_i and χ_e arise from uncertainties in the respective convective multipliers. The values of χ_i are shown only for $r/a > 0.3$ for the coinjection case since convection strongly dominates the transport for $r/a \leq 0.3$. As seen in Fig. 3, $\chi_i(r)$ has a magnitude and radial dependence comparable to that of $\chi_e(r)$, which agrees with the results from the T_i simulations shown in Fig. 1. For comparison, the range of the values of χ_i^{NC} derived from neoclassical theory is also shown in Fig. 3(a), and is seen to deviate strongly from the range of values deduced from the kinetic measurements.

The thermal diffusivities themselves are not significantly different between cases of balanced and unbalanced injection. The observed differences in the ion-temperature profiles are apparently explained by taking into account the downshift of beam energies in the rotating plasma frame, a mild broadening of the beam-deposition profile, and the occurrence of off-axis ion heating due to viscous rotational damping.

The authors wish to thank K. Young, R. Hawryluk, D. Meade, the TFTR operations staff, and the TFTR technical crew for support during this work. This work was supported by U.S. DOE Contract No. DE-AC02-76-CH0-3073.

[a]Permanent address: Los Alamos National Laboratory, Los Alamos, NM 87544.

[1]H. Eubank *et al.*, Phys. Rev. Lett. **43**, 270 (1979).

[2]G. Becker *et al.*, Nucl. Fusion **23**, 1293 (1983).

[3]D. W. Swain *et al.*, Nucl. Fusion **21**, 1409 (1981).

[4]S. M. Kaye *et al.*, Nucl. Fusion **24**, 1303 (1984).

[5]R. J. Groebner *et al.*, Nucl. Fusion **26**, 543 (1986).

[6]M. Okabayashi *et al.*, in *Proceedings of the Eleventh International Conference on Plasma Physics and Controlled Nuclear Fusion Research, 13–20 November 1986, Kyoto, Japan,* edited by J. W. Weiland and M. Demir (IAEA, Vienna, 1987), p. 275.

[7]J. D. Strachan *et al.*, Phys. Rev. Lett. **58**, 1004 (1987).

[8]M. Bitter *et al.*, Plasma Phys. Controlled Fusion **29**, 1235 (1987).

[9]R. B. Howell, R. Fonck, K. Jaehnig, and R. Knize, Rev. Sci. Instrum. **59**, 1521 (1988).

[10]R. J. Fonck *et al.*, in *Proceedings of the Fifteenth European Conference on Controlled Fusion and Plasma Physics, 16–20 May 1988, Dubrovnik,* edited by S. Pesic and J. Jacquinot (European Physical Society, Petit-Lancy, 1988), p. I-83.

[11]C. J. Chang and F. L. Hinton, Phys. Fluids **25**, 1493 (1982).

[12]M. C. Zarnstorff *et al.*, in Proceedings of the Twelfth International Conference on Plasma Physics and Controlled Nuclear Fusion Research, 12–19 October 1988, Nice, France (to be published).

[13]M. C. Zarnstorff *et al.*, in Ref. 10, p. I-95; Plasma Phys. Controlled Fusion (to be published).

[14]R. J. Goldston, in *Basic Physical Processes of Toroidal Fusion Plasmas,* edited by G. P. Lampis *et al.* (Commission of the European Communities, Brussels, 1986), Vol. 1, p. 165.

[15]S. Scott *et al.*, in Ref. 12.